Energy Engineering

Tech Science Press

Doi:10.32604/ee.2025.072333

ARTICLE

Multi-Timescale Coordinated Optimal Dispatch of Active Distribution Networks Incorporating Thermal Storage Electric Heating Clusters

Song Zhang, Yang Yu*, Shuguang Li and Xue Li

School of Electrical Engineering, Northeast Electric Power University, Jilin, 132012, China

*Corresponding Author: Yang Yu. Email: 2202300131@neepu.edu.cn

Received: 24 August 2025; Accepted: 09 October 2025; Published: 27 February 2026

ABSTRACT: Thermal storage electric heating (TSEH), as a prevalent variable load resource, offers significant potential for enhancing system flexibility when aggregated into a cluster. To address the uncertainties of renewable energy and load forecasting in active distribution networks (ADN), this paper proposes a multi-timescale coordinated optimal dispatch strategy that incorporates TSEH clusters. It utilizes the thermal storage characteristics and short-term regulation capabilities of TSEH, along with the rapid and gradual response characteristics of resources in active distribution grids, to develop a coordinated optimization dispatch mechanism for day-ahead, intraday, and real-time stages. It provides a coordinated optimized dispatch technique across several timescales for active distribution grids, taking into account the integration of TSEH clusters. The proposed method is validated on a modified IEEE 33-node system. Simulation results demonstrate that the participation of TSEH in collaborative optimization significantly reduces the total system operating cost by 8.71% compared to the scenario without TSEH. This cost reduction is attributed to a 10.84% decrease in interaction costs with the main grid and a 47.41% reduction in network loss costs, validating effective peak shaving and valley filling. The multi-timescale framework further enhances economic efficiency, with overall operating costs progressively decreasing by 3.91% (intraday) and 4.59% (real-time), and interaction costs further reduced by 5.34% and 9.25%, respectively. Moreover, the approach enhances system stability by effectively suppressing node voltage fluctuations and ensuring all voltages remain within safe operating limits during real-time operation. Therefore, the proposed approach achieves rational coordination of diverse resources, significantly improving the economic efficiency and stability of ADNs.

KEYWORDS: Active distribution network; thermal storage electric heating; distributed energy resources; rolling optimization; multiple time scales

1 Introduction

To better meet the “dual carbon” targets, State Grid Corporation of China is actively pushing clean heating policies. It suggests replacing conventional heating methods like coal-fired boilers with electric heating and other alternatives to ensure the environment’s sustainable growth [1]. Large-scale connections of electric heating equipment to the power grid, however, could put the system’s stability and safety at risk due to unexpected spikes in peak loads, decreased line operating efficiency, and node voltage exceeding limits as the “coal-to-electricity” project advances swiftly [2]. Thermal storage electric heating (TSEH) introduces a heat storage device based on electric heating, achieving combined heating and heat storage operation with a certain degree of heat storage regulation capability [3]. After cluster aggregation, it may participate in grid demand response as a dispatchable load resource, effectively performing peak shaving and valley filling [4].

Thus, researching the TSEH cluster scheduling mechanism is crucial for enhancing power system flexibility and promoting the effective use of clean energy.

Cluster scheduling for electric heating loads has been extensively studied by both domestic and foreign researchers. In [5], a control strategy for residential electric heating loads has been suggested, which includes ground-source heat pumps and air-source heat pumps, with the goal of improving the economic efficiency of residential heating. In [6], in order to guarantee both the steady operation of the power grid and the effective operation of electric boilers, a multiple start-stop operation strategy for TSEH is suggested when interfacing with the grid. In [7], a deep reinforcement learning-based multi-agent cooperative optimization control framework is developed to optimize supply and demand matching in electric heating systems. In [8], a dual-layer optimization and model predictive control based heat load management plan is developed for community energy systems, achieving reliable and economical scheduling through coordinated operator-user benefit optimization. In [9], an optimal control strategy for TSEH is developed, incorporating user thermal comfort preferences quantified via maximum likelihood estimation to balance operational economy with grid peak-shaving demands. In [10], intelligent TSEH load control is demonstrated to simultaneously optimize electricity retailer profits and user costs, effectively enhancing grid load-tracking capability. In [11], a grid safety-constrained optimal dispatch model for TSEH is established, effectively reducing operational costs while mitigating distribution grid load impacts. In [12], an optimal integration of electric heat pumps with medium-scale thermal storage is shown to maximize wind power utilization, whereas oversized storage degrades system efficiency, demanding a balanced configuration for optimal performance.

At the same time, traditional distribution grids are increasingly changing into active distribution networks (ADN) due to the widespread use of active management tools including distributed power generation, flexible loads, and large-scale energy storage [13–16]. But because of their high degree of unpredictability and volatility, renewable energy sources provide major difficulties for system dispatch choices and raise operational uncertainty in the distribution grid [17]. Enhancing dispatch plans' capacity to adjust to the unpredictability of renewable energy generation is now a popular area of research. In [18], a multi-timescale coordinated dispatch method is developed for ADN, employing two-stage (day-ahead/intraday) optimization and intelligent soft switch-EV coordination to enhance operational efficiency under uncertainty. Cone relaxation and two-stage robust optimization are used in [19] to efficiently reduce ADN losses under wind power uncertainty by coordinating discrete/continuous reactive power compensation devices. In [20], a two-stage robust dispatch strategy is developed, incorporating time-of-use pricing and distributed generation reactive power regulation to minimize total supply costs. In [21], a multi-timescale scheduling framework is established, harmonizing demand response with user satisfaction through two-stage day-ahead/real-time optimization. This approach effectively mitigates distributed generation power fluctuations while enhancing distribution grid operational efficiency. It is obvious that ADN can efficiently integrate various distributed resources to achieve comprehensive regulation. This interaction not only enhances the economic viability and operational efficiency of each distributed resource but also strengthens the system stability and economic benefits of ADN.

The cluster scheduling of TSEH and the operational control of ADN have been covered in the previously stated literature, however there is still a lack of study in the following areas:

(1) From the perspective of resource aggregation and dispatch, existing research predominantly treats electric heating loads as user-side control objects, focusing on optimization for individual users or localized groups. It has yet to treat aggregated TSEH as a dispatchable resource from an ADN perspective for rational allocation, thereby achieving optimal operation in terms of both stability and economy.

(2) The short-term regulatory potential of TSEH for mitigating load prediction variation and renewable energy variability is not sufficiently explored in current research.
(3) System flexibility is severely limited by the understudied complementary coordination between TSEH and active management devices in ADN, especially when viewed through multi-timescale perspectives.

The paper proposes multi-timescale coordinated optimum dispatch of ADN utilizing TSEH clusters to overcome the aforementioned problems. The thermal conversion and heat storage properties of TSEH systems, as well as the operational variations of different active regulatory devices within the ADN across various time scales, form the basis of this approach. The multi-stage cooperative coordination between TSEH systems and customizable resources inside the ADN is fully taken into account. This approach achieves a sensible distribution of power resources across various time scales by utilizing the flexibility of the TSEH system and the resources on the ADN side. It successfully improves the ADN system's economic performance and operational efficiency, and real-world case studies support the suggested scheduling approach.

2 Multi-Time Scale Collaborative Optimization Scheduling Framework

To reduce the uncertainty of renewable energy generation in ADN and the impact of demand forecast errors on system scheduling, fine-grained scheduling may be achieved by progressively reducing the time scale. This will increase the rationality of ADN optimized scheduling by making the optimized scheduling results more consistent with the actual system operation [22]. Based on the thermal storage characteristics and short-term regulation capabilities of TSEH, this paper establishes a multi-timescale collaborative optimization dispatch framework for ADN incorporating heat storage electric heating clusters. During the day-ahead planning phase, it participates as a dispatchable resource in formulating economic dispatch plans, determining heat storage and release rhythms, and providing decision-making foundations for slow-response equipment. In the intraday and real-time phases, it fully leverages its short-term power regulation capabilities, coordinating with fast-response resources such as micro-gas turbines and energy storage systems to jointly mitigate renewable energy output fluctuations and load forecast deviations. This multi-timescale coordination enables the thermal storage electric heating cluster to optimize system economic operation at the macro level while simultaneously tracking power fluctuations in real time at the micro level. Fig. 1 illustrates the collaborative optimal scheduling framework and ADN multi-time scale coordination relationship developed in this article, taking into account TSEH cluster access.

Using hourly resolution, optimization choices must be taken during the recent scheduling phase based on electric heating load demand, renewable energy output, and system factors (grid structure and electricity pricing data) within a 24-h forecast cycle. Due to mechanical inertia restrictions, slow-response equipment like on-load tap changers (OLTC) and capacitor banks (CB) in active distribution grids are unable to react rapidly to minute-level dispatch orders. Consequently, it is necessary to ascertain their operating state during this dispatch period. Furthermore, centralized management of TSEH is developed in order to fulfill the thermal demand of heating users. Plans for thermal storage and heat release are created specifically for TSEH, and the outcomes of each dispatch optimization are sent to the intraday phase.

Information on electricity/heat load demand, projection data for renewable energy generation, and other pertinent data must be acquired four hours prior to the intraday scheduling phase. With updates every hour, the schedule plan is created on a 15-min time frame. Rolling optimization is used to determine the output of the rapid regulation equipment (energy storage system (ESS), micro-turbine (MT)) in the ADN, and the intraday baseline operating power of the TSEH system. Based on the results of the day-ahead optimization and the intraday system operating limitations, the outcomes of each schedule optimization are subsequently sent to the real-time stage.

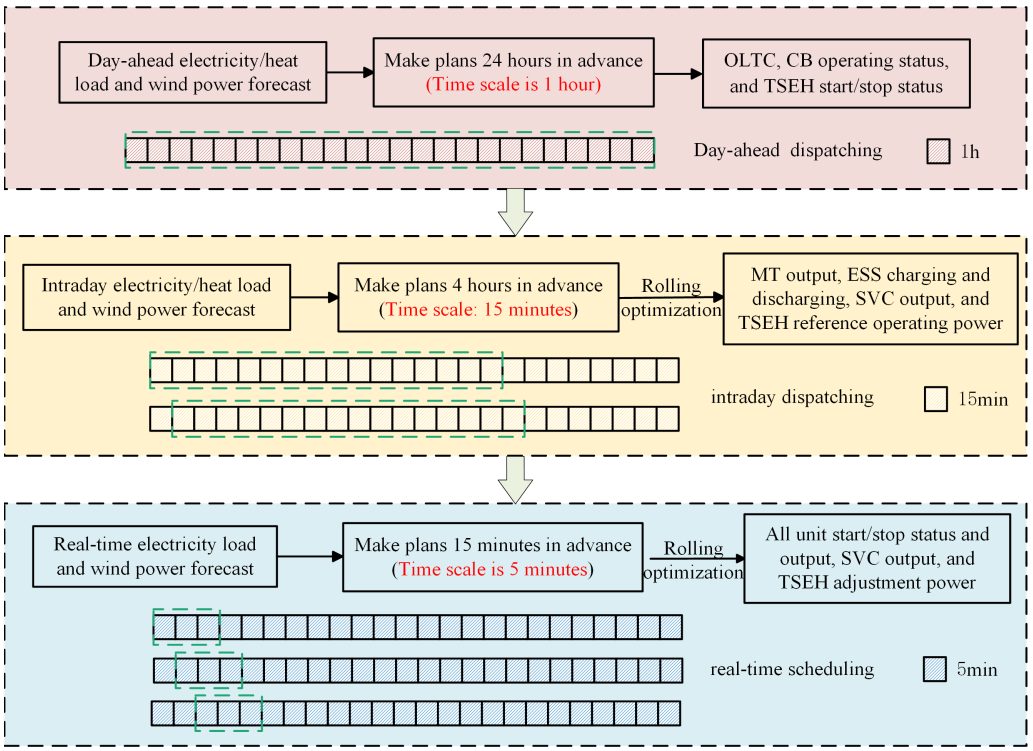

Figure 1: Multi-time-scale coordination and collaborative optimization scheduling framework

A 15-min time scale is enough to satisfy heating demands during real-time scheduling because of the comparatively moderate thermal reaction. As a result, with electricity scheduling done on a 5-min time frame, forecast data for renewable energy output and electrical load demand only has to be obtained 15 min in advance. In order to avoid additional costs associated with repeated charging and discharging of ESS equipment, the ESS output values determined by the intraday scheduling plan are also implemented immediately in this phase. Considering the outcomes of the day-ahead intraday optimization and system operating constraints, this phase determines the output and start/stop status of every unit, the output adjustment of static var compensators (SVC), and the real-time correction power of TSEH.

3 Multi-Time Scale Collaborative Optimization Scheduling Model

3.1 Day-Ahead Optimization Scheduling Model

3.1.1 Objective Function

The day-ahead optimization scheduling model predicts the production of new energy sources and the demand for electricity and heat load based on previous operational data and day-ahead weather forecasts. The goal is to reduce ADN's overall operational expenses throughout the course of the scheduling cycle. While ensuring the thermal comfort of electric heating users, the output of each slow-response device in ADN and the day-ahead scheduling plan are determined. Here is the objective function:

$$\min F_1 = C_{MT} + C_{Loss} + C_{ESS} + C_{grid} \tag{1}$$

where the current period T = 24 h, and the time resolution is 1 h. The specific calculation methods for each part are described below.

(1) Operating costs of MT

$$C_{\mathrm{MT}} = \sum_{t=1}^{T} \sum_{i=1}^{N_g} \left[\rho_{\mathrm{MT},i} P_{\mathrm{MT}i,t} \right] \tag{2}$$

where C_{MT} is the operating costs of MT; N_g is the total MT count in ADN; $P_{\mathrm{MT}i,t}$ represents the active power output of the i^{th} MT at time t; $\rho_{\mathrm{MT},i}$ represents the i^{th} MT's marginal operating cost.

(2) Distribution network loss costs

$$C_{\mathrm{Loss}} = \sum_{t=1}^{T} \sum_{ij} r_{ij} I_{ij,t}^2 \alpha_t \tag{3}$$

where C_{Loss} is total network loss cost of the distribution network; r_{ij} is the branch circuit resistance between node i and node j; $I_{ij,t}$ is the effective value of the current in the corresponding branch at time t; α_t is the cost of energy loss per unit, i.e., network loss electricity price.

(3) ESS dispatch costs

$$C_{\mathrm{ESS}} = \sum_{t=1}^{T} \sum_{i=1}^{N_e} \alpha_{\mathrm{ess}} \left(P_{\mathrm{char},i,t} + P_{\mathrm{dis},i,t} \right) \tag{4}$$

where C_{ESS} is ESS dispatch costs; N_e is the number of ESS devices within ADN; α_{ess} is the ESS unit dispatch cost coefficient; The i^{th} ESS device's charging and discharging powers at time t are denoted by $P_{\mathrm{char},i,t}$ and $P_{\mathrm{dis},i,t}$, respectively.

(4) Interaction electricity cost with the upper-level power grid

$$C_{\mathrm{grid}} = \sum_{t=1}^{T} c_{\mathrm{g},t} P_{\mathrm{g},t} \tag{5}$$

where C_{grid} is ADN and upper grid interaction electricity costs; $c_{\mathrm{g},t}$ is main grid electricity price at time t; The interaction power between the upper-level power grid and ADN over time t is denoted by $P_{\mathrm{g},t}$.

3.1.2 Constraints

(1) Electric power balance constraint

$$\sum_{i}^{N_g} P_{\mathrm{MT}i,t} + \sum_{i}^{N_{dg}} P_{\mathrm{wt}i,t} + P_{\mathrm{g},t} + P_{\mathrm{dis},t} = P_{\mathrm{char},t} + P_{\mathrm{load},t} + \sum_{m=1}^{N_m} P_{\mathrm{EH}m,t} \tag{6}$$

$$Q_{\mathrm{g},t} + Q_{\mathrm{CB},t} + Q_{\mathrm{SVC},t} = Q_{\mathrm{load},t} \tag{7}$$

where $P_{\mathrm{load},t}$, $Q_{\mathrm{load},t}$ are active and reactive power in the ADN at time t, respectively; $Q_{\mathrm{g},t}$ is the reactive power supplied by the higher grid at time t; $Q_{\mathrm{CB},t}$ is the reactive power injected by the CB grouped and switched at time t; $Q_{\mathrm{SVC},t}$ is the reactive power supplied by the SVC device at time t; $P_{\mathrm{EH}m,t}$ is the power consumption of the m^{th} TSEH device at time t.

(2) Constraints on heating balance for households with electric heating

Considering the thermal inertia of electric heating systems, operational complexity can be reduced by making sure that, without rigorously adhering to real-time power balance, the total heat supply during the scheduling cycle matches user heat demand while still satisfying actual heating requirements. According

to the principles of building thermodynamics, the heating balance constraints for user buildings can be expressed as:

$$\sum_{\Delta t}^{T}\left(H_{\mathrm{eh},t}+H_{\mathrm{S},t}-H_{\mathrm{A},t}-H_{\mathrm{V},t}-H_{\mathrm{b},t}\right)=\sum_{\Delta t}^{T}C_{\mathrm{air}}T_{\mathrm{in},t} \tag{8}$$

where C_{air} is the equivalent thermal capacity of the building's air; $T_{\mathrm{in},t}$ is the heating user's interior temperature at time t; $H_{\mathrm{eh},t}$ is the heating power that the TSEH system provides to the building over time t; $H_{\mathrm{S},t}$ is the radiant heat provided to the building by sunlight at time t; $H_{\mathrm{A},t}$ is the conductive heat transferred from the indoor to the outdoor environment through the building at time t; $H_{\mathrm{V},t}$ is the dissipation of heat in both indoor and outdoor air at time t; $H_{\mathrm{b},t}$ is the building's heat loss due to thermal inertia at time t; Δt is a 1-h time scale; The scheduling cycle T is 24 h. The relevant heat calculation formulas for each part are as follows [23]:

$$H_{\mathrm{A},t}=H_{\mathrm{wall},t}+H_{\mathrm{window},t} \tag{9}$$

$$H_{\mathrm{wall},t}=\left[T_{\mathrm{in},t}-T_{\mathrm{out},t}\right]k_{\mathrm{wall}} \tag{10}$$

$$H_{\mathrm{window},t}=\left[T_{\mathrm{in},t}-T_{\mathrm{out},t}\right]k_{\mathrm{window}} \tag{11}$$

$$H_{V,t}=vk_{v}\left[T_{in,t}-T_{out,t}\right] \tag{12}$$

$$H_{\mathrm{S},t}=M_{\mathrm{S}}F_{\mathrm{W}} \tag{13}$$

$$H_{\mathrm{b},t}=\left(T_{\mathrm{in},t}-T_{\mathrm{in},t-1}\right)L_{\mathrm{b}}VC_{\mathrm{b}}/\tau \tag{14}$$

where $H_{\mathrm{wall},t}$ and $H_{\mathrm{window},t}$ represent the heat loss of the building's exterior walls and windows, respectively, at time t; $T_{\mathrm{out},t}$ is the outdoor temperature at time t; k_{wall} and k_{window} are the heat transfer coefficients of the building's exterior walls and windows, respectively; v is the outdoor wind speed; k_{v} is the overall heat transfer coefficient; M_{S} stands for the intensity of solar radiation; F_{W} is the building's equal daylighting area; L_{b} is the building's overall density; V is the volume of the building; C_{b} is the building's specific thermal capacity; τ is the time constant of thermal inertia.

(3) Constraints on the working characteristics of TSEH

Under ideal circumstances, TSEH technology simultaneously provides real-time heating and heat storage during off-peak grid periods, ensuring steady grid operation and minimizing heating costs for consumers [24]; The system mainly uses the thermal storage unit to provide heating during periods of high grid load, with electric heating units acting as a complement. By moving peak loads to off-peak times and lowering customers' heating expenses through off-peak energy prices, this strategy preserves grid stability and lessens the operational strain brought on by the system's integration of distributed renewable power sources.

1. TSEH power constraints

$$P_{\mathrm{EH},t}=\left(P_{\mathrm{eh},t}+P_{\mathrm{abs},t}\right)B_{\mathrm{abs},t} \tag{15}$$

where $P_{\mathrm{EH},t}$ is total power consumption for TSEH at time t; $P_{\mathrm{eh},t}$ is the direct heating power for TSEH at time t; $P_{\mathrm{abs},t}$ is the amount of electricity used by the heat storage device at time t; $B_{\mathrm{abs},t}$ is the heat storage status of TSEH at time t.

2. TSEH thermal power balance constraints

$$H_{\mathrm{eh},t}=\eta_{0}P_{\mathrm{eh},t}B_{\mathrm{abs},t}+H_{\mathrm{relea},t}B_{\mathrm{relea},t} \tag{16}$$

where η_0 is the energy efficiency coefficient of direct heating mode for TSEH; $H_{\mathrm{relea},t}$ is the heat storage device's release of heat power at time t; $B_{\mathrm{relea},t}$ is the heat release state of the heat storage device at time t.

3. Constraints on the heat storage characteristics of TSEH

$$S_{\mathrm{eh},t+1} = S_{\mathrm{eh},t}\left(1-\mu\right) + \left(\eta^{\mathrm{abs}} P_{\mathrm{abs},t} - H_{\mathrm{relea},t}\right)\Delta t \tag{17}$$

where $S_{\mathrm{eh},t}$ is the heat storage device's ability to store heat at time t; μ is the self-consumption energy coefficient of heat storage device; η^{abs} is the heat storage efficiency of heat storage devices; Δt is the scheduling interval.

(4) Constraints on the operation of TSEH

Heating power, heat storage power, heat release power, and higher and lower restrictions on the heat storage device's capacity are the primary constraints for TSEH. For single-unit TSEH devices, heat storage and heat release cannot occur simultaneously, and the initial and final heat storage levels in the scheduling cycle should remain consistent:

$$\begin{cases} 0 \le P_{\mathrm{eh},t} \le P_{\mathrm{eh}}^{\max} \\ 0 \le P_{\mathrm{abs},t} \le P_{\mathrm{abs}}^{\max} \\ 0 \le P_{\mathrm{relea},t} \le P_{\mathrm{relea}}^{\max} \\ B_{\mathrm{abs},t} + B_{\mathrm{relea},t} \le 1 \\ S_{\mathrm{eh,t0}} = S_{\mathrm{eh,T}} \\ S_{\mathrm{eh}}^{\min} \le S_{\mathrm{eh},t} \le S_{\mathrm{eh}}^{\max} \end{cases} \tag{18}$$

where $P_{\mathrm{eh}}^{\max}$, $P_{\mathrm{abs}}^{\max}$ and $P_{\mathrm{relea}}^{\max}$ are the maximum power limits for direct heating, heat storage, and heat release in TSEH systems; $S_{\mathrm{eh},t0}$ and $S_{\mathrm{eh,T}}$ are the heat storage device's starting and ultimate capacities during the scheduling cycle, respectively; $S_{\mathrm{eh}}^{\min}$ and $S_{\mathrm{eh}}^{\max}$ are the lowest and highest allowable heat storage capacities of the unit, respectively.

TSEH should have some regulatory authority to rectify the imbalance brought on by inaccurate wind and load forecasts:

$$\begin{cases} \Delta P_{\mathrm{EH},t}^{u} = \sum\limits_{m=1}^{N_m} P_{\mathrm{EH}m,t}^{\max} - \sum\limits_{m=1}^{N_m} P_{\mathrm{EH}m,t} \\ \Delta P_{\mathrm{EH},t}^{d} = \sum\limits_{m=1}^{N_m} P_{\mathrm{EH}m,t} \end{cases} \tag{19}$$

where: $\Delta P_{\mathrm{EH},t}^{u}$ and $\Delta P_{\mathrm{EH},t}^{d}$ are TSEH's capacity for both upward and downward adjustment at time t, respectively.

TSEH can only reduce power while it is operating at full load; it is unable to boost power. Reasonably controlling the system's output power and maintaining the required adjustment margin are essential to guaranteeing that it has enough adjustment space while operating:

$$\begin{cases} \sum\limits_{m=1}^{N_m} P_{\mathrm{EH}m,t} \le \sum\limits_{m=1}^{N_m} P_{\mathrm{EH}m,t}^{\max} - P_{\mathrm{EH},t}^{up} \\ P_{\mathrm{EH},t}^{up} = \lambda_{up} \sum\limits_{m=1}^{N_m} P_{\mathrm{EH}m,t}^{\max} \end{cases} \tag{20}$$

where $P_{\mathrm{EH},t}^{up}$ is the reserved upward adjustment power margin for TSEH at time t; λ_{up} is the TSEH power reserve coefficient.

(5) Operational constraints of MT

$$\begin{cases} P_{\mathrm{MT}}^{\min} \le P_{\mathrm{MT},t} \le P_{\mathrm{MT}}^{\max} \\ \Delta P_{\mathrm{MT}}^{\min} \le P_{\mathrm{MT},t} - P_{\mathrm{MT},t-1} \le \Delta P_{\mathrm{MT}}^{\max} \end{cases} \tag{21}$$

where $P_{\mathrm{MT}}^{\min}$ and $P_{\mathrm{MT}}^{\max}$ are the lower and upper limits of the output of MT, respectively; $\Delta P_{\mathrm{MT}}^{\max}$ and $\Delta P_{\mathrm{MT}}^{\min}$ are the upper and lower limits of active power ramping for MT.

(6) Distributed power supply output constraints

With the following constraints, this article analyzes ADN operational characteristics under dispersed wind power grid connection conditions:

$$P_{\mathrm{wt}}^{\min} \le P_{\mathrm{wt},t} \le P_{\mathrm{wt}}^{\max} \tag{22}$$

where: $P_{\mathrm{wt}}^{\min}$ and $P_{\mathrm{wt}}^{\max}$ are the lowest and highest possible power generation from the wind turbine, respectively.

(7) Operational constraints of ESS

$$\begin{cases} E_{t+1}^{\mathrm{ESS}} = E_t^{\mathrm{ESS}} + \eta_{\mathrm{char}} P_{\mathrm{char},t} - P_{\mathrm{dis},t}/\eta_{\mathrm{dis}} \\ 0 \le P_{\mathrm{char},t} \le P_{\mathrm{char},t,\max} \\ 0 \le P_{\mathrm{dis},t} \le P_{\mathrm{dis},t,\max} \\ E_{\min}^{\mathrm{ESS}} \le E_t^{\mathrm{ESS}} \le E_{\max}^{\mathrm{ESS}} \\ E_{t0}^{\mathrm{ESS}} = E_T^{\mathrm{ESS}} \\ u_{\mathrm{char},t} + u_{\mathrm{dis},t} \le 1 \end{cases} \tag{23}$$

where E_t^{ESS} is the state of charge of ESS at time t; η_{char} and η_{dis} are charging and discharging efficiency of ESS, respectively; $P_{\mathrm{char}}^{\max}$ and $P_{\mathrm{char}}^{\min}$ are ESS charging and discharging power upper and lower limits; $E_{\min}^{\mathrm{ESS}}$ and $E_{\max}^{\mathrm{ESS}}$ are ESS state of charge upper and lower limits, respectively; E_{t0}^{ESS} and E_T^{ESS} are ESS storage capacity at the beginning and end of the scheduling cycle, respectively; $u_{\mathrm{char},t}$ and $u_{\mathrm{dis},t}$ represent the charging and discharging states of the ESS, respectively, and are Boolean variables. Charging and discharging operations of the ESS cannot be performed simultaneously.

(8) Operational constraints of OLTC

$$\begin{cases} V_{m,t} = k_{\mathrm{OLTC},t} V_{j.t} \\ k_{\mathrm{OLTC},t} = k_{\mathrm{OLTC}}^{\min} + S_{\mathrm{OLTC},t} \dfrac{k_{\mathrm{OLTC}}^{\max} - k_{\mathrm{OLTC}}^{\min}}{N_{\mathrm{OLTC}}} \end{cases} \tag{24}$$

where $V_{m,t}$ is the voltage value of node j after conversion by OLTC; $k_{\mathrm{OLTC},t}$ is the OLTC tap ratio at t moment; $k_{\mathrm{OLTC}}^{\min}$ and $k_{\mathrm{OLTC}}^{\max}$ are minimum and maximum tap ratios for OLTC, respectively; $S_{\mathrm{OLTC},t}$ is the OLTC tap sequence at time t; N_{OLTC} is the total number of OLTC tap positions.

(9) Constraints on group switching of CB

$$\begin{cases} Q_{\mathrm{CB},t} = N_{\mathrm{CB},t} Q_{\mathrm{CB},t}^{\mathrm{step}} \\ N_{\mathrm{CB},t} \le N_{\mathrm{CB},t}^{\max} \\ T_{\mathrm{CB},t} \le \left| N_{\mathrm{CB},t+1} - N_{\mathrm{CB},t} \right| \le T_{\mathrm{CB},t} Q_{\mathrm{CB},t}^{\mathrm{step}} \\ \sum_{t=1}^{T} T_{\mathrm{CB},t} \le T_{\mathrm{CB,max}} \end{cases} \tag{25}$$

where $N_{\mathrm{CB},t}$ and $N_{\mathrm{CB},t}^{\max}$ are the capacitor bank switch position and the main switch position, respectively; $Q_{\mathrm{CB},t}^{\mathrm{step}}$ is the single-stage switching capacity of CB; $T_{\mathrm{CB},t}$ is the operating status of CB; $T_{\mathrm{CB,max}}$ is the maximum operating frequency of CB during dispatching periods.

(10) Operational constraints of SVC

$$Q_{\mathrm{SVC}}^{\min} \le Q_{\mathrm{SVC},t} \le Q_{\mathrm{SVC}}^{\max} \tag{26}$$

where $Q_{\mathrm{SVC}}^{\min}$ and $Q_{\mathrm{SVC}}^{\max}$ are the SVC compensation power's bottom and upper bounds, respectively; To mitigate reverse power flow and overvoltage issues in distribution networks due to high distributed generation penetration, this paper sets the lower limit $Q_{\mathrm{SVC}}^{\min}$ of SVC reactive power compensation to a negative value [25].

(11) Interaction power constraints with the upper-level power grid

$$P_{\mathrm{g},t}^{\min} \le P_{\mathrm{g},t} \le P_{\mathrm{g},t}^{\max} \tag{27}$$

where $P_{\mathrm{g},t}^{\min}$ and $P_{\mathrm{g},t}^{\max}$ are the power interchange boundaries (lower/upper) for ADN-main network interaction, respectively.

(12) ADN trend constraint

$$\begin{cases} P_i = U_i \sum_{j=1}^{N} U_j \left(G_{ij} \cos\theta_{ij} + B_{ij} \sin\theta_{ij} \right) \\ Q_i = U_i \sum_{j=1}^{N} U_j \left(G_{ij} \cos\theta_{ij} - B_{ij} \sin\theta_{ij} \right) \end{cases} \tag{28}$$

where: P_i and Q_i are the active and reactive power injected into the nodes, respectively; The voltages for nodes i and j are denoted by U_i and U_j, respectively; G_{ij}, B_{ij}, θ_{ij} are the conductance, admittance, and phase angle difference of the voltage between nodes i and j, respectively.

(13) ADN operational safety constraints

$$\begin{cases} U_{\min} \le U_{i,t} \le U_{\max} \\ I_{ij,t} \le I_{ij}^{\max} \end{cases} \tag{29}$$

where $U_{\min}$ and $U_{\max}$ are the upper and lower voltage limits for system nodes; $I_{ij}^{\max}$ is the maximum current that the circuit allows to flow.

3.2 Intraday Optimization Scheduling Model

3.2.1 Objective Function

The previous day's plan serves as the basis for intraday scheduling, which accounts for the demand for electricity and heat load as well as short-term wind power output estimates. In order to lower the overall running costs of the ADN during the scheduling period, a rolling optimization scheduling model is

developed for the intraday phase. In order to increase the precision of scheduling optimization and decrease the discrepancy between the previous day's scheduling plan and actual operating conditions, this model calculates the output of each rapid-response device within the ADN system, the output of MT units, and the base power of the TSEH. Building elements like windows and outside walls absorb heat through heating equipment because of the thermal inertia of buildings, but the internal temperature takes time to climb to the desired level. This research uses the same 15-min time scale as electrical energy scheduling for thermal energy scheduling during the intraday period in order to better handle the time lag difficulties in heat transmission and control on the user side. In order to improve the system's regulation precision, this time scale selection complements the ADN's quick regulation resources and efficiently takes into account the dynamic changes in heat energy transfer and interior temperature regulation. The proposed objective function:

$$\min F_2 = C'_{\mathrm{MT}} + C'_{\mathrm{Loss}} + C'_{\mathrm{ESS}} + C'_{\mathrm{grid}} + C_{\mathrm{EH}} \tag{30}$$

where the superscript "$\prime$" represents the comprehensive operating cost of ADN during the intraday dispatching phase; TSEH costs are covered by CEH and are determined using Eq. (31).

$$C_{\mathrm{EH}} = k_{\mathrm{EH}} \sum_{m=1}^{M} \left| P_{\mathrm{EH}m,t} - P'_{\mathrm{EH}m,t} \right| \tag{31}$$

where k_{EH} is the TSEH power adjustment compensation cost coefficient; $P'_{\mathrm{EH}m,t}$ represents the power consumption of TSEH intraday.

3.2.2 Constraints

The limitations of the intraday phase are simplified by the intraday rolling optimization scheduling phase as the operational parameters and output of OLTC and CB have already been determined in the day-ahead scheduling plan. The ADN-related operational limitations, TSEH constraints, and output constraints for each fast-response device in the ADN are the same as those in day-ahead optimization scheduling and will not be discussed here:

3.3 Real-Time Optimization Scheduling Model

3.3.1 Objective Function

In order to minimize system operating costs, the real-time scheduling phase combines ultra-short-term wind power output and load demand forecast data. Each power generation unit's output deviation compensation costs are taken into account, and the operating power of the TSEH and the output of the SVC are continuously adjusted to fulfill the goal of measuring power fluctuations in real-time. The objective function is as follows:

$$\min F_3 = C^{\mathrm{RT}}_{\mathrm{MT}} + C^{\mathrm{RT}}_{\mathrm{Loss}} + C^{\mathrm{RT}}_{\mathrm{ESS}} + C^{\mathrm{RT}}_{\mathrm{grid}} + C_{\mathrm{EH}} + C_{\mathrm{TZ}} \tag{32}$$

$$\begin{cases} C_{\mathrm{EH}} = k_{\mathrm{EH}} \sum\limits_{m=1}^{M} \left| P'_{\mathrm{EH}m,t} - P^{\mathrm{RT}}_{\mathrm{EH}m,t} \right| \\ C_{TZ} = \omega^{tz}_{\mathrm{MT}} \sum\limits_{i=1}^{N_g} \left| P'_{\mathrm{MT}i,t} - P^{\mathrm{RT}}_{\mathrm{MT}i,t} \right| + \omega^{tz}_{\mathrm{g}} \sum\limits_{i=1}^{N_g} \left| P'_{\mathrm{grid},t} - P^{\mathrm{RT}}_{\mathrm{grid},t} \right| \end{cases} \tag{33}$$

where the superscript "RT" represents the comprehensive operating cost of ADN during the real-time scheduling phase; $P^{\mathrm{RT}}_{\mathrm{EH}m,t}$ is the total power consumption optimized by TSEH for the real-time phase; C_{TZ} calculates the deviation cost for dispatchable resources in the real-time phase; $\omega^{tz}_{\mathrm{MT}}$ and ω^{tz}_{g} represent the

unit deviation costs for MT and interactive electricity, respectively, where $\omega_{\mathrm{MT}}^{tz}$ is 0.63 CNY/kWh and ω_{g}^{tz} is the main grid electricity price.

3.3.2 Constraints

The output constraints of each fast-response device in the ADN included in the model, the TSEH constraints, and the operational constraints associated to the ADN are identical to those in the day-ahead optimization scheduling during the real-time scheduling phase, thus they won't be repeated here. The power regulation limits should be met in this phase as TSEH can be freely modified in accordance with the operational power benchmark established during the intraday phase:

$$\Delta P_{\mathrm{EH},t}^{d} \leq \sum_{m=1}^{M} \Delta P_{\mathrm{EH}m,t} \leq \Delta P_{\mathrm{EH},t}^{u} \tag{34}$$

where $\Delta P_{\mathrm{EH}m,t}$ provides real-time power adjustment for TSEH during the t time period.

4 Case Study Analysis

4.1 Calculation Example System and Parameter Settings

This paper uses an improved IEEE 33-node distribution network for case study analysis, as follows: the system reference voltage is 10 kV, the range of the node voltage tolerance is 0.94 to 1.06 p.u., the three-phase power reference value is 10 MVA, and the diagram of the network topology is displayed in Fig. 2. The parameters for each device in the ADN are listed in the Appendix A, Tables A1–A7. A typical daily outdoor temperature variation curve is shown in Appendix Fig. A1. For detailed Parameters for the thermodynamic model of typical residential buildings, see Appendix Table A8. The main grid electricity price adopts a time-of-use pricing model, with time periods divided as shown in Table 1 [26]. The optimization model constructed in this paper can be modeled using the YALMIP platform and solved using the GUROBI commercial solver.

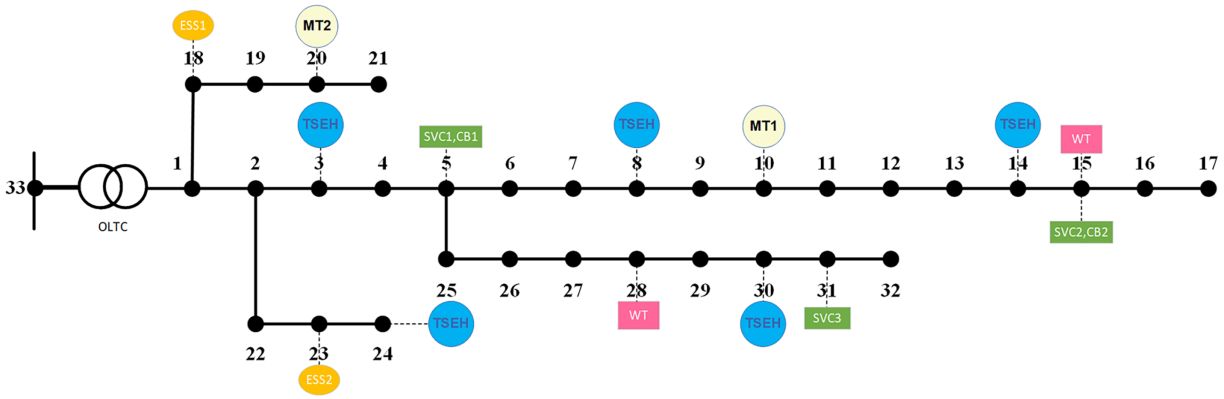

Figure 2: The topology of modified IEEE-33 node active distribution network

In this research, joint prediction curves for wind power and load at several time scales are constructed by superimposing normally distributed errors. The day-ahead, intraday, and real-time dispatch phases have confidence ranges of ±20%, ±5%, and ±2% for wind power output forecasts, respectively. For load forecasts, the relevant confidence intervals are set at ±3%, ±1%, and ±0.5%. The resulting prediction curves are shown in Fig. 3.

Table 1: Time-of-use tariff information

Time period division	Type	Electricity price/ (yuan/kWh)
(9:00 a.m. to 12:00 p.m. and 5:00 p.m. to 8:00 p.m.)	Peak section	0.834
(7:00 a.m.–9:00 a.m., 12:00 p.m.–5:00 p.m., and 8:00 p.m.–10:00 p.m.)	Flat section	0.648
(10:00 p.m. to 12:00 a.m. and 12:00 a.m. to 7:00 a.m.)	Valley section	0.463

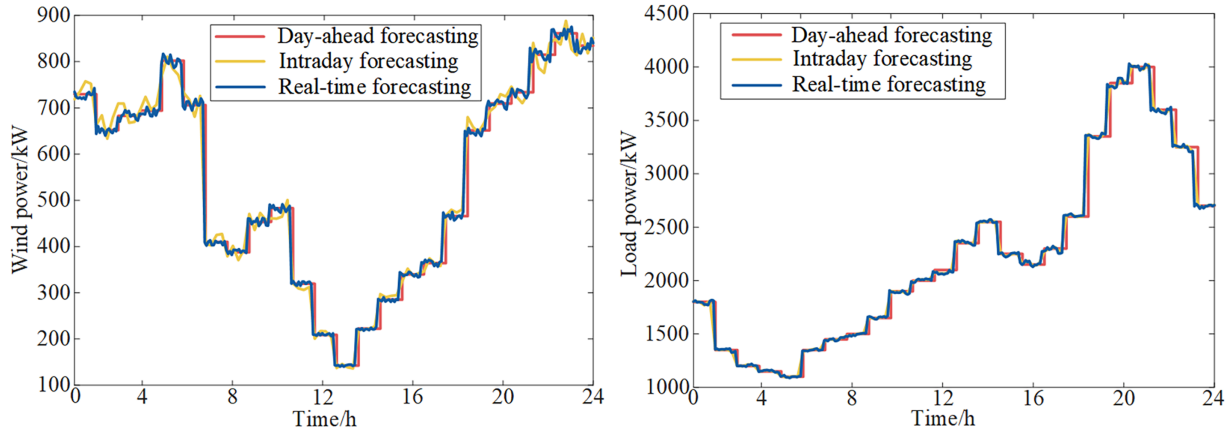

Figure 3: Wind power and load forecast curves

4.2 Analysis of Day-Ahead Scheduling Results

The day-ahead optimization of wind power forecast power and various active management measures is integrated to formulate a dispatch plan. The active power output of each dispatch resource on the day-ahead is shown in Fig. 4.

As seen in Fig. 4, the TSEH system is turned on for heat storage during typical off-peak electrical consumption times (such as 0:00–06:00), which raises the overall load power. The TSEH heating system shuts off during typical high power usage times (such as 17:00–20:00), and the heat storage system constantly releases stored heat for heating, ensuring that indoor temperatures are maintained to satisfy user heating needs; For MT, since its marginal operating cost is lower than the peak-off-peak electricity price but higher than the off-peak electricity price, and the output of distributed wind farms is relatively low during the 11:00–17:00 period, MT operates during peak-off-peak periods to reduce the active distribution grid's electricity purchase costs during peak periods and alleviate grid pressure; For ESS, energy is stored during the low-cost off-peak hours at night and released during the peak midday hours, which not only lowers the grid's electricity purchase expenses but also effectively balances the grid's supply and demand relationship.

Reactive power resources within the ADN may be modified to maintain node voltages within a manageable range during the day-ahead dispatch phase, preventing node voltage from exceeding distribution network limitations when wind turbine production is too high or demand is too heavy. The intraday phase then receives the OLTC's tap settings and the number of CB switching groups. Following the completion of the day-ahead dispatch plan, Fig. 5 displays the OLTC's tap settings and the number of CB switching groups.

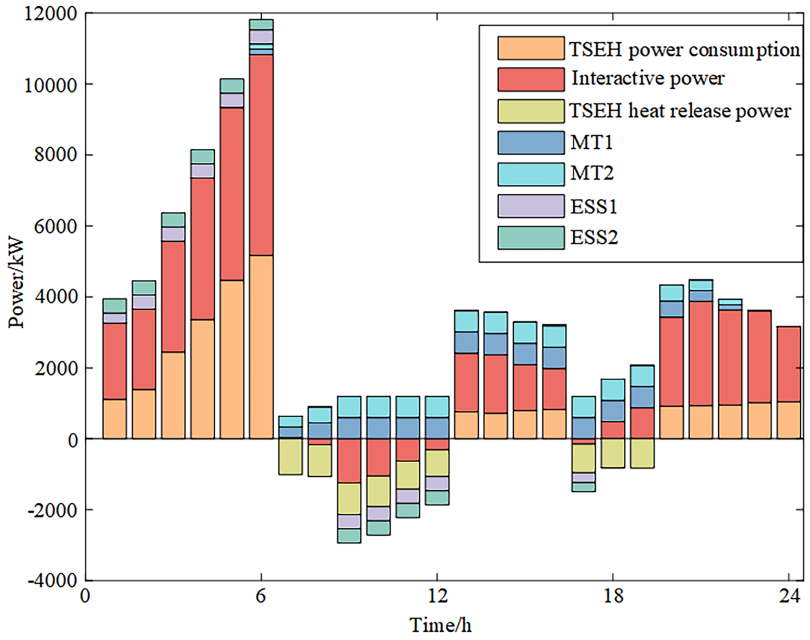

Figure 4: Day-ahead active power output of dispatching resources

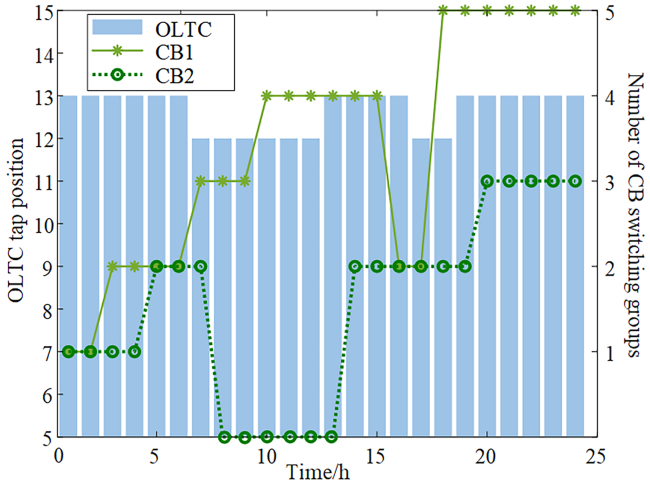

Figure 5: Tap Position of OLTC and Switching Groups of CB

Fig. 6 shows the dispatch results when TSEH is not involved in the collaborative optimization of the Active Distribution Network (ADN). To further demonstrate the synergistic optimization effect, we also conducted a comparative analysis in Fig. 7 of the voltage distribution across ADN nodes before and after TSEH's involvement in scheduling. Additionally, Fig. 8 provides a voltage profile comparison to more clearly illustrate the temporal trends in voltage magnitude.

Analysis results indicate that if large-scale electric heating users concentrate heat storage between 02:00 and 05:00, then rely on heat release to maintain heating from 06:00 to 21:00, this approach may reduce user energy costs but would increase ADN's electricity procurement costs from the main grid. It would also exacerbate node voltage fluctuations, adversely affecting system operational stability. By implementing

the proposed TSEH-participating coordinated optimization dispatch strategy, TSEH loads are rationally regulated across the time dimension. This approach not only effectively smooths the system's net load curve but also significantly suppresses voltage fluctuations, improves voltage quality, and enhances both the operational stability and economic efficiency of ADN.

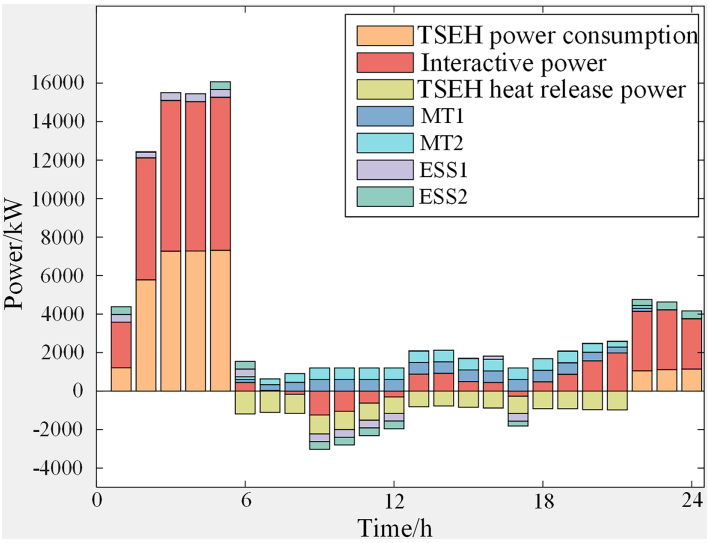

Figure 6: TSEH does not participate in ADN optimized scheduling results

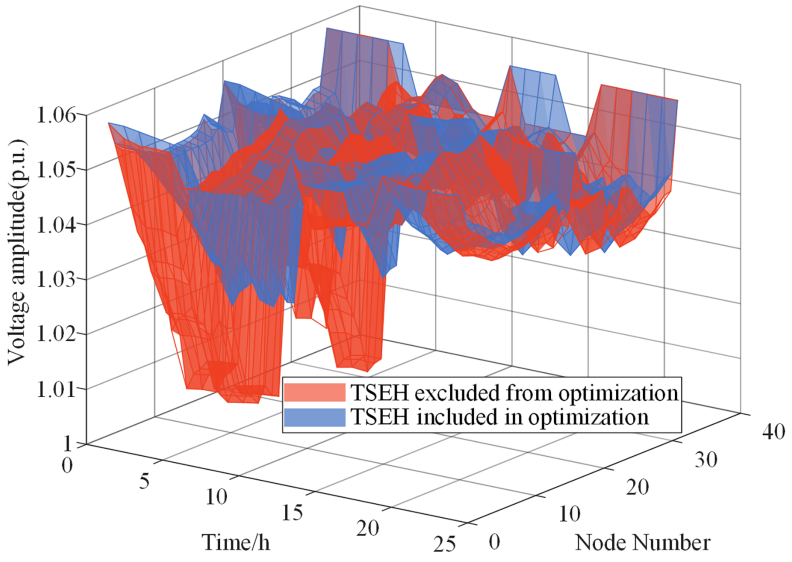

Figure 7: TSEH participation in optimizing pre- and post-node voltage changes

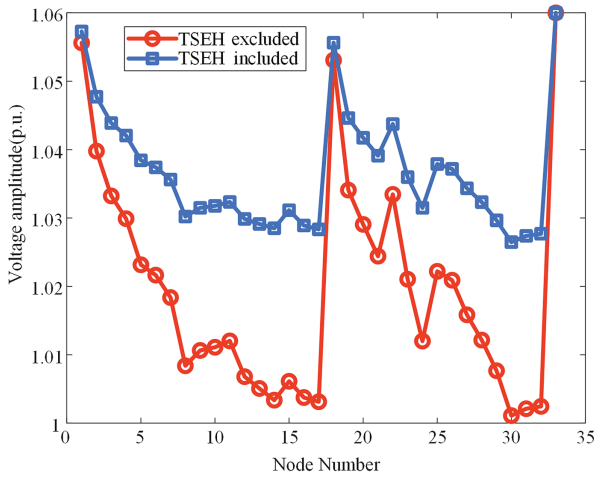

(a) Figure 7: 5:00 Profile

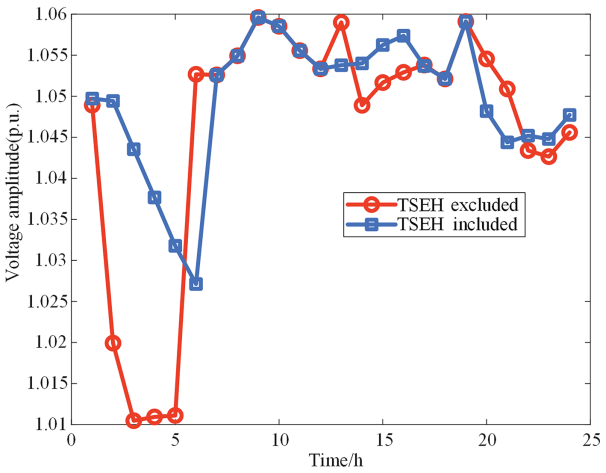

(b) Figure 7: Cross-section at Node 10

Figure 8: Fig. 7 Cross-section at 5:00 and Node 10

4.3 Analysis of Intraday Scheduling Results

The TSEH benchmark electricity load taking part in ADN collaborative optimization, MT output, ESS output, and interaction electricity with the upper-level power grid are among the scheduling items for the day. Following intraday rolling optimization, Fig. 9 displays each resource's output.

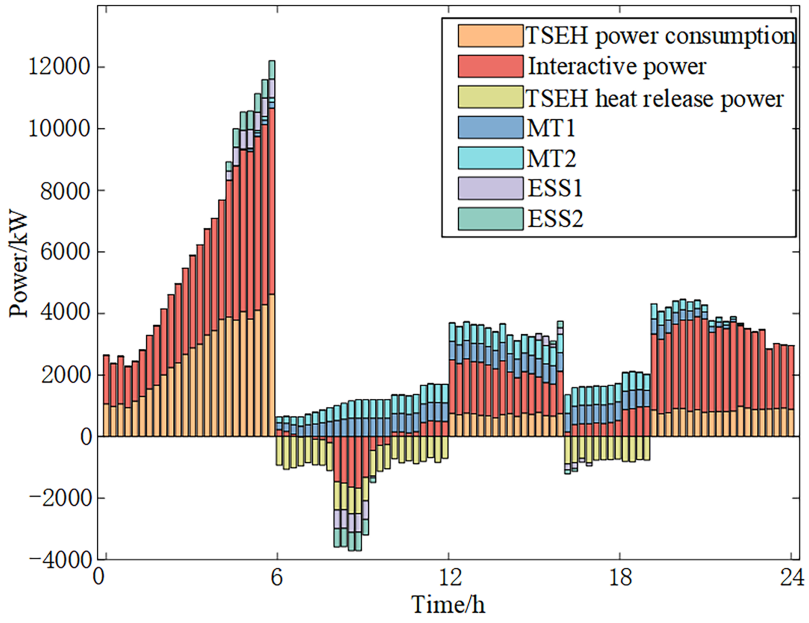

Figure 9: Intraday output status of dispatchable Resources

Fig. 9 illustrates that MT's operational trend is consistent with the day before. The TSEH cluster load uses its rapid regulation capabilities based on the start-stop status established the day before to ensure heating while calculating the baseline operating power and transmitting it to the real-time phase in order to mitigate power imbalance issues brought on by variations in WT output and load. Its limited regulatory capabilities,

however, mean that in order to achieve the requirements for dependable and cost-effective system operation, cooperation with ESS and MT within the distribution network is required.

4.4 Analysis of Real-Time Scheduling Results

Real-time dispatch objects include TSEH load adjustment, SVC output adjustment, and interaction with the upper-level power grid. Through dynamic correction of the daily plan, both system economy and regulation accuracy are optimized. During the real-time dispatch phase, the dispatch status of each dispatch resource is shown in Fig. 10.

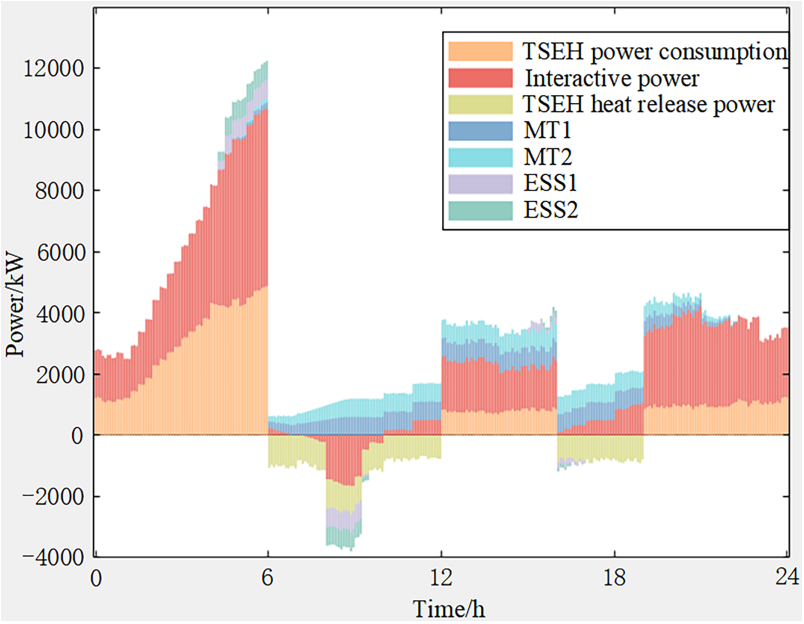

Figure 10: Real-time output status of dispatchable resources

The system's capacity to follow WT random variations much increases when the scheduling cycle is shorter, as seen in Figs. 9 and 10. By integrating real-time rolling optimization with a dynamic feedback mechanism, the system flexibly modifies active power output during the real-time scheduling phase, efficiently reducing power deviations brought on by WT variations and guaranteeing the power grid's steady operation.

The voltage distribution (normalized values) for every system node during the real-time scheduling stage is displayed in Fig. 11. For the ADN to continue operating steadily, the node voltage values' magnitude is essential. While low node voltages can cause system failures and lower power supply dependability, excessively high node voltages can cause equipment overload and decreased energy efficiency. All node voltages, as depicted in the figure, stay within the system's safe operating range, confirming that the technique suggested in this work can guarantee the ADN's dependable and steady operation.

Compare the operating costs of ADN in the four scheduling phases, as shown in Table 2.

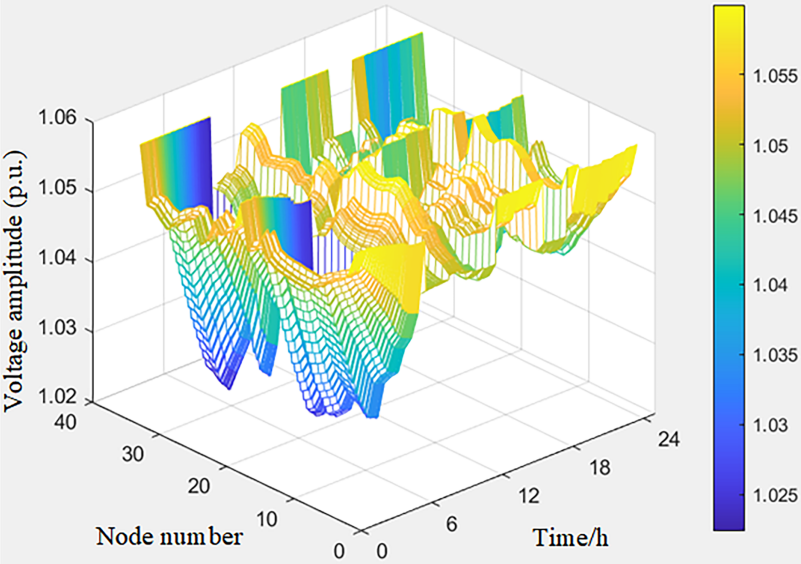

Figure 11: Real-time phase node voltage distribution

Table 2: Optimization results of operation cost

Scheduling phase	Interaction costs (RMB)	Network loss costs (RMB)	MT operating costs (RMB)	ESS scheduling costs (RMB)	Compensate costs (RMB)	Variance costs (RMB)	Total costs (RMB)
TSEH does not participate in scheduling.	21,419.67	602.88	10,569.83	433.02	0	0	33,025.40
Day-ahead	19,098.48	317.08	10,583.99	418.54	0	0	30,148.09
Intraday	18,078.33	302.88	10,300.57	278.89	268.02	0	29,228.69
Real-time	17,332.21	301.83	10,250.41	278.89	111.43	747.56	29,022.33

As shown in Table 2, when TSEH is not involved in optimization scheduling, the total system operating cost is 33,025.40 yuan. After TSEH participates in collaborative optimization, the total system operating cost is significantly reduced to 30,148.09 yuan, representing a decrease of 8.71%. This cost reduction stems primarily from two factors: First, interaction costs with the main grid decreased from 21,419.67 yuan to 19,098.48 yuan, a 10.84% reduction. This indicates that by rationally scheduling TSEH's heat storage and discharge behavior, effective "peak shaving and valley filling" was achieved, reducing electricity purchases from the main grid. Second, grid loss costs decreased from RMB 602.88 to RMB 317.08, a reduction of 47.41%. This reflects more rational power flow distribution within the system following optimized scheduling, resulting in significantly lower line losses. At the same time, by analyzing the results of operational cost optimization across three phases—day-ahead, intraday, and real-time, during the intraday optimization and real-time rectification schedule stages, it is evident that the system's TSEH compensation costs and system deviation costs increased compared to the day-ahead phase. However, while the overall operating costs of the ADN reduced by 3.91% and 4.59%, respectively, the interaction costs with the upper-level grid decreased

by 5.34% and 9.25%. Therefore, by taking into account TSEH cluster access, the multi-timescale coordinated optimization strategy for ADN operation suggested in this paper can rationally coordinate TSEH load with the operational states of different active management devices, increasing the efficiency of distribution grid equipment and resource utilization. Consequently, this lowers the exorbitant price of buying power and improves the stability and economic efficiency of the system.

5 Conclusions

In order to fully utilize the control capabilities of the TSEH cluster and achieve optimal allocation and efficient utilization of system resources, this paper suggests an ADN multi-timescale collaborative optimization scheduling strategy that takes into account TSEH cluster access. This approach addresses the problems of strong output fluctuations and low prediction accuracy in the context of high proportions of renewable energy access. The method was validated using an upgraded IEEE 33-node system, and the following conclusions were drawn:

(1) Peak shaving and valley filling may be accomplished efficiently by utilizing TSEH's scheduling capabilities to the fullest extent feasible and allowing it to take part in the coordinated optimization of ADN operations, which will reduce the operating strain on the distribution network.

(2) By building a multi-time-scale collaborative decision-making framework with "day-ahead, intraday, and real-time" scales, the suggested solution fully utilizes TSEH's quick reaction capabilities to track and gradually optimize the fluctuation of renewable energy output. In addition to improving system scheduling accuracy, it suggests the best scheduling schemes for resources with distinct response characteristics across several control phases, balancing the needs for power supply dependability and system economic operation.

Acknowledgement: The authors wish to express their gratitude to the National Natural Science Foundation of China for its financial support of this technology management project.

Funding Statement: This work is supported by Integrated Distribution Network Planning and Operational Enhancement Using Flexibility Domains Under Deep Human-Vehicle-Charger-Road-Grid Coupling (U22B20105).

Author Contributions: The authors confirm contribution to the paper as follows: Conceptualization, Song Zhang and Yang Yu; methodology, Song Zhang; validation, Song Zhang, Yang Yu and Shuguang Li; formal analysis, investigation, resources and data curation, Song Zhang and Yang Yu; writing—original draft preparation, Song Zhang, Yang Yu and Shuguang Li; writing—review and editing, Xue Li; visualization and supervision, Song Zhang and Xue Li. All authors reviewed the results and approved the final version of the manuscript.

Availability of Data and Materials: The authors confirm that the data supporting the findings of this study are available within the article.

Ethics Approval: Not applicable.

Conflicts of Interest: The authors declare no conflicts of interest to report regarding the present study.

Nomenclature

Optimization Variables

$P_{\mathrm{MT}i,t}$	Active power output of the ith MT at time t
$I_{ij,t}$	Effective value of the current in the corresponding branch at time t
$P_{\mathrm{char},i,t}$	The ith ESS device's charging powers at time t
$P_{\mathrm{dis},i,t}$	The ith ESS device's discharging powers at time t
$P_{\mathrm{g,t}}$	The interaction power between the upper-level power grid and ADN at time t
$Q_{\mathrm{g},t}$	Reactive power supplied by the higher grid at time t

$Q_{\mathrm{CB},t}$	Reactive power injected by the CB grouped and switched at time t
$Q_{\mathrm{SVC},t}$	Reactive power supplied by the SVC device at time t
$P_{\mathrm{EH}m,t}$	Power consumption of the mth TSEH device at time t
$T_{\mathrm{in},t}$	Heating user's interior temperature at time t
$H_{\mathrm{eh},t}$	Heating power that the TSEH system provides to the building over time t
$P_{\mathrm{EH},t}$	Total power consumption for TSEH at time t
$P_{\mathrm{eh},t}$	Direct heating power for TSEH at time t
$P_{\mathrm{abs},t}$	Amount of electricity used by the heat storage device at time t
$B_{\mathrm{abs},t}$	Heat storage status of TSEH at time t
$H_{\mathrm{relea},t}$	Heat storage device's release of heat power at time t
$B_{\mathrm{relea},t}$	Heat release state of the heat storage device at time t
$S_{\mathrm{eh},t}$	Heat storage device's ability to store heat at time t
$\Delta P^{u}_{\mathrm{EH},t}$	TSEH's capacity for upward adjustment at time t
$\Delta P^{d}_{\mathrm{EH},t}$	TSEH's capacity for downward adjustment at time t
E^{ESS}_{t}	State of charge of ESS at time t
$u_{\mathrm{char},t}$	Charging states of the ESS at time t
$u_{\mathrm{dis},t}$	Discharging states of the ESS at time t
$k_{\mathrm{OLTC},t}$	OLTC tap ratio at t moment
$N_{\mathrm{CB},t}$	Capacitor bank switch position at time t
$T_{\mathrm{CB},t}$	Operating status of CB at time t
$P^{'}_{\mathrm{EH}m,t}$	Power consumption of TSEH intraday
$P^{'}_{\mathrm{MT}i,t}$	Active power output of the ith MT intraday
$P^{'}_{\mathrm{grid},t}$	The interaction power between the upper-level power grid and ADN intraday
$P^{\mathrm{RT}}_{\mathrm{EH}m,t}$	Power consumption optimized by TSEH for the real-time phase
$P^{\mathrm{RT}}_{\mathrm{MT}i,t}$	Active power output of the ith MT for the real-time phase
$P^{\mathrm{RT}}_{\mathrm{grid},t}$	The interaction power between the upper-level power grid and ADN for the real-time phase

Appendix A

Table A1: Parameters of OLTC

Installation node	Adjustment range	Gear
33-1	0.94~1.06 p.u.	13

Table A2: Parameters of MT

Installation node	Rated capacity/KVA	Climbing rate	Unit marginal cost/(yuan/kWh)
10, 20	600	1/4	0.63

Table A3: Parameters of ESS

Installation node	Upper capacity limits/MWh	Lower capacity limits/kWh	Maximum charge and discharge power/kW	The charge/discharge efficiency	Unit dispatch cost/(yuan/kWh)
18, 23	2.4	300	400	0.95	0.05

Table A4: Parameters of CB

Installation node	Rated capacity/kvar	Capacity per group/kvar
5, 15	500	100

Table A5: Parameters of SVC

Installation node	Rated capacity/kvar
5, 15, 31	700

Table A6: Parameters of WT

Installation node	Installed capacity/MW
15, 28	1

Table A7: Parameters of TSEH

Installation node	3, 8, 14, 24, 30
Number of households connected to each node	100
Heating device efficiency ratio/(%)	95
Heat storage efficiency of heat storage devices/(%)	90
Maximum heating power/kW	5
Maximum heat storage capacity/kW	8
Maximum heat release power/kW	8
Self-consumption energy coefficient/(%)	2
Compensation cost coefficient/(yuan/kWh)	0.14

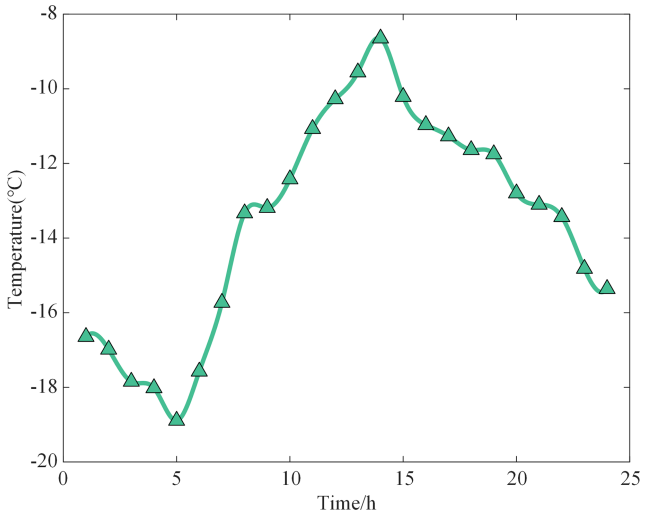

Figure A1: A typical daily outdoor temperature variation curve

Table A8: Parameters for the thermodynamic model of typical residential buildings

Parameters	Numerical value
k_{wall}	18
k_{window}	21
$v/(m\ s^{-1})$	3.2
$M_S/(W\ m^{-2})$	156
F_W/m^2	7
k_v	12.1
$C_{air}/(W\ h/°C)$	3.2025
$L_b/(kg/m^3)$	1800
$C_b/(J/(kg°C))$	840
τ	18

References

1. Wang W, Li F. Study on substitutable value of electric heating instead of coal heating in northern China under carbon constraints. J Clean Prod. 2020;260(1):121155. doi:10.1016/j.jclepro.2020.121155.
2. Xu J, Wang F, Li B, Xiang C, Su N, Zhang Z. Optimal configuration of regenerative electric heating for improving distribution network carrying capacity. In: Proceedings of the 2024 IEEE 8th Conference on Energy Internet and Energy System Integration (EI2); 2024 Nov 29–Dec 2; Shenyang, China. p. 3398–403. doi:10.1109/EI264398.2024.10991436.
3. Guo J, Yu J, Wang Y, Zhang X. Experimental study on air source heat pump heating system based on phase change heat storage. IEEE Access. 2023;11:110878–87. doi:10.1109/ACCESS.2023.3321916.
4. Yang D, Li B, Liu G, Sun Y, Fu J, Liu C. A flexibility assessment method of thermal storage electric heating load clusters. In: Proceedings of the 2022 IEEE 6th Conference on Energy Internet and Energy System Integration (EI2); 2022 Nov 11–13; Chengdu, China. p. 538–42. doi:10.1109/EI256261.2022.10117130.
5. Zhang S, Cheng H, Wang D, Zhang L, Li F, Yao L. Distributed generation planning in active distribution network considering demand side management and network reconfiguration. Appl Energy. 2018;228:1921–36. doi:10.1016/j.apenergy.2018.07.054.
6. Reynders G, Amaral Lopes R, Marszal-Pomianowska A, Aelenei D, Martins J, Saelens D. Energy flexible buildings: an evaluation of definitions and quantification methodologies applied to thermal storage. Energy Build. 2018;166:372–90. doi:10.1016/j.enbuild.2018.02.040.
7. Shen R, Zhong S, Zheng R, Yang D, Xu B, Li Y, et al. Advanced control framework of regenerative electric heating with renewable energy based on multi-agent cooperation. Energy Build. 2023;281:112779. doi:10.1016/j.enbuild.2023.112779.
8. Jin X, Wu Q, Jia H, Hatziargyriou ND. Optimal integration of building heating loads in integrated heating/electricity community energy systems: a bi-level MPC approach. IEEE Trans Sustain Energy. 2021;12(3):1741–54. doi:10.1109/TSTE.2021.3064325.
9. Guan D, Feng Z, Song L, Hu K, Li Z, Ye P. An optimal operation strategy of regenerative electric heating considering the difference in user thermal comfort. Energies. 2023;16(15):5821. doi:10.3390/en16155821.
10. Kilkki O, Alahäivälä A, Seilonen I. Optimized control of price-based demand response with electric storage space heating. IEEE Trans Ind Inform. 2015;11(1):281–8. doi:10.1109/TII.2014.2342032.
11. Xuejun S, Shupeng L, Xianxu H, Jie S, Weiguo Z. Research on optimal dispatching strategy of regenerative electric heating in critical safety state of power grid. In: Proceedings of the 16th IET International Conference on AC and DC Power Transmission (ACDC 2020); 2020 Jul 2–3; Online. p. 556–62.

12. Wang H, Han J, Zhang R, Sun M, Sun Z, Hua P, et al. Heat-power peak shaving and wind power accommodation of combined heat and power plant with thermal energy storage and electric heat pump. Energy Convers Manag. 2023;297(5):117732. doi:10.1016/j.enconman.2023.117732.
13. Verzijlbergh RA, De Vries LJ, Lukszo Z. Renewable energy sources and responsive demand: do we need congestion management in the distribution grid? IEEE Trans Power Syst. 2014;29(5):2119–28. doi:10.1109/TPWRS.2014.2300941.
14. Gaurav A, Tyagi A, Jha SK, Kumar B. Optimal sizing and economic assessment of grid connected active distribution network for reliable rural electrification in India. Energy Convers Manag. 2024;311:118505. doi:10.1016/j.enconman.2024.118505.
15. Dutta R, Chakrabarti S, Sharma A. Topology tracking for active distribution networks. IEEE Trans Power Syst. 2021;36(4):2855–65. doi:10.1109/TPWRS.2020.3045855.
16. Prasad M, Rather ZH, Razzaghi R, Doolla S. A new approach to determine feasible operating region of unbalanced distribution networks with distributed photovoltaics. IEEE Trans Power Deliv. 2025;40(3):1493–504. doi:10.1109/TPWRD.2025.3555210.
17. Zheng W, Huang W, Hill DJ, Hou Y. An adaptive distributionally robust model for three-phase distribution network reconfiguration. IEEE Trans Smart Grid. 2021;12(2):1224–37. doi:10.1109/TSG.2020.3030299.
18. Yang X, Xu C, Zhang Y, Yao W, Wen J, Cheng S. Real-time coordinated scheduling for ADNs with soft open points and charging stations. IEEE Trans Power Syst. 2021;36(6):5486–99. doi:10.1109/TPWRS.2021.3070036.
19. Ding T, Liu S, Yuan W, Bie Z, Zeng B. A two-stage robust reactive power optimization considering uncertain wind power integration in active distribution networks. IEEE Trans Sustain Energy. 2015;7(1):301–11. doi:10.1109/TSTE.2015.2494587.
20. Zhang J, Cui M, He Y, Li F. Multi-period two-stage robust optimization of radial distribution system with cables considering time-of-use price. J Mod Power Syst Clean Energy. 2022;11(1):312–23. doi:10.35833/mpce.2021.000283.
21. Sheng H, Wang C, Li B, Liang J, Yang M, Dong Y. Multi-timescale active distribution network scheduling considering demand response and user comprehensive satisfaction. IEEE Trans Ind Appl. 2021;57(3):1995–2005. doi:10.1109/TIA.2021.3057302.
22. Chen S, Wang C, Zhang Z. Multitime scale active and reactive power coordinated optimal dispatch in active distribution network considering multiple correlation of renewable energy sources. IEEE Trans Ind Appl. 2021;57(6):5614–25. doi:10.1109/TIA.2021.3100468.
23. Feng YC, Jia HP, Yan M, Li GZ, Liu L, Liu DN. Operation optimization method for virtual power plant participating in clean heating based on time-of-use tariff of wind power. Electr Power. 2024;57(1):51–60. (In Chinese). doi:10.11930/j.issn.1004-9649.202306102.
24. Lei Z, Wang G, Li T, Cheng S, Yang J, Cui J. Strategy analysis about the active curtailed wind accommodation of heat storage electric boiler heating. Energy Rep. 2021;7(2):65–71. doi:10.1016/j.egyr.2021.02.021.
25. Gao HJ, Liu JY, Shen XD, Xu R. Optimal power flow research in active distribution network and its application examples. Proc CSEE. 2017;37(6):1634–45. (In Chinese). doi:10.13334/j.0258-8013.pcsee.152839.
26. Niu YF, Feng TY, Wang CF, Sha ZC, Xu DP. Multi-time scale optimal dispatching method of active distribution network considering the influence of cycle life for energy storage system. Electr Power Constr. 2024;45(11):89–101. (In Chinese). doi:10.12204/j.issn.1000-7229.2024.11.008.